Towards a Realistic Theoretical Electronic Spectra of Metal Aqua Ions in Solution: The Case of Ce(H2O)n3+ Using Statistical Methods and Quantum Chemistry Calculation

Gema Raposo-Hernández, Rafael Pappalardo, Florent Réal, Valérie Vallet, Enrique Sánchez Marcos

Towards a Realistic Theoretical Electronic Spectra of Metal Aqua Ions in Solution: The Case of $Ce(H_2O)_n^{3+}$ Using Statistical Methods and Quantum Chemistry Calculations

Gema Raposo-Hernández,[1] Rafael R. Pappalardo,[1] Florent Réal,[2] Valérie Vallet,[2] and Enrique Sánchez Marcos[1]

[1)] *Department of Physical Chemistry, University of Seville, 41012-Seville, Spain*

[2)] *Université de Lille, CNRS, UMR 8523-PhLAM, Physique des Lasers, Atomes et Molecules, F-59000 Lille, France*

(*Electronic mail: sanchez@us.es)

(Dated: 13 September 2024)

Accurately predicting spectra for heavy elements, often open-shell systems, is a significant challenge typically addressed using a single cluster approach with a fixed coordination number. Developing a realistic model that accounts for temperature effects, variable coordination numbers, and interprets experimental data is even more demanding due to the strong solute-solvent interactions present in solutions of heavy metal cations. This study addresses these challenges by combining multiple methodologies to accurately predict realistic spectra for highly-charged metal cations in aqueous media, with a focus on the electronic absorption spectrum of Ce^{3+} in water. Utilizing highly correlated relativistic quantum mechanical (QM) wavefunctions and structures from molecular dynamics (MD) simulations, we show that the convolution of individual vertical transitions yields an excellent agreement with experimental results without the introduction of empirical broadening. The good results are obtained for both the normalized spectrum and that of absolute intensity. The study incorporates a statistical machine learning algorithm, Gaussian Mixture Models-Nuclear Ensemble Approach (GMM-NEA), to convolute individual spectra. The microscopic distribution provided by MD simulations allows us to examine the contributions of the octa- and ennea-hydrate of Ce^{3+} in water to the final spectrum. Additionally, the temperature dependence of the spectrum is theoretically captured by observing the changing population of these hydrate forms with temperature. We also explore an alternative method for obtaining statistically representative structures in a less demanding manner than MD simulations, derived from QM Wigner distributions. The combination of Wigner-sampling and GMM-NEA broadening shows promise for wide application in spectroscopic analysis and predictions, offering a computationally efficient alternative to traditional methods.

PACS numbers: Valid PACS appear here

Keywords: Ce^{3+} hydrate, classical interaction potentials, MD, NEVPT2, electronic transitions, statistical average of transitions, line broadening procedures

I. INTRODUCTION

Ultraviolet–visible (UV-vis) spectroscopy is a widely used characterization technique due to the distinctive features it provides, such as the position and spacing of the luminescence bands, their bandwidths and intensities, serving as unique fingerprints for compounds and complexes absorbing in the UV-vis region[1–7]. This method has proven valuable for studying ion speciation in electrolyte solutions, as the local environment strongly influences the electronic structure[8]. However, in certain cases, spectroscopic information alone may not fully determine sample properties.

From a theoretical perspective, various approaches offer insights into spectrum properties. Quantum mechanical (QM) calculations have long contributed to a better understanding of recorded spectra features and the underlying physics of excitation processes. Techniques such as time-dependent density functional theory (TD-DFT) or high-level iterative such as Equation of Motion Coupled-Cluster Theory (EOM-CCSD(T)) and multi-reference methods like Complete Active Space Self-Consistent Field (CASSCF) and the second-order perturbation theory such as CASPT2 or NEVPT2 (N-Electron Valence Perturbation Theory of the Second Order) methods, etc., have successfully described the luminescence of many systems[9–12]. These computations yield information about transition energies and intensities. However, to construct the full picture of electronic spectrum, an additional ingredient is needed: signal broadening.

Achieving signal broadening using a single structure is a challenging task. Various strategies have been adopted to address this challenge. One approach involves deriving the band shape from the autocorrelation function between the ground state and time-dependent excited-state wave functions[13,14], computing the spectral band shapes from the vibronic coupling of the electronic states. Oher *et al.*[15] computed integrals between vibrational wave functions associated with the ground and excited states, known as Franck-Condon factors (FCFs). In many cases, FCF calculations use the harmonic approximation; however, Barone *et al.*[16–18] went further by including anharmonic corrections via vibrational perturbation theory (VPT2). Chang, Chen, and Huang[19] used a similar strategy with a different approach to include anharmonicity in the FCF calculations. Madsen *et al.*[20] considered only an a priori selected small number of normal modes. These strategies are accurate and often provide a good reproduction of the experimental spectra but are computationally demanding.

Alternative methods for obtaining band shapes extend beyond dealing with a single structure and rely on an ensemble of configurations. The broadening of the band can result from convoluting individual energies and oscillator strengths with a typically assigned phenomenological broadening[11,21]. These ensembles can be derived from statistical simulations, either classical or ab initio[11,22–24], which encompass all anharmonicities in their description. Another widely used technique, the Wigner sampling method[25,26], utilizes normal vibrational modes to generate different structures from the potential energy surface minimum of the target system[27,28]. This approach eliminates the need for a force field or expensive ab initio molecular dynamics but operates under a harmonic description, so it may struggle with low-frequency modes or highly flexible systems. More sophisticated methods, such as the one proposed by Cerezo *et al.*[29,30], couple Molecular Dynamics (MD) for the exploration of the configurational space and vibronic models for the band shapes, eliminating the need for phenomenological broadening. Another approach described by Segarra-Martí *et al.*[14] also combines classical sampling and quantum mechanical tools to compute electronic spectra with a QM broadening of the bands. The strategy is to consider the physical origin of the broadening (intra-molecular vibrations, homogeneous and inhomogeneous broadening) and model these different contributions to obtain the final spectrum.

These studies commonly focus on molecules that, even in solution, maintain a consistent structure. The investigation of metal ions in solution is particularly intriguing, because anharmonicities could significantly impact in the representation of a flexible metal complex dynamics, especially concerning the first-shell water molecules and structural changes in the aqua ion. Modifications in ligand orientations, distances, and even coordination number can influence the electronic structure to some extent[8]. Some of the works already cited above emphasize the importance of including solvent effects, both implicitly or explicitly, for more realistic modeling of absorption spectra[11,22,24,30,31]. Not just for a more accurate description of the dynamics of the system, but for a better description of the electronic structure when there are strong solute-solvent interactions in the explicit solvent models. In this context, the review by Zuehlsdorff and Isborn[11] presents representative examples on how electronic spectra of solutions such as Nile red in acetone and ethanol[32], or cyanin in water[33,34] can be well described by including solvent effects at the molecular level.

This study aims to compute the UV-visible absorption spectrum of the Ce^{3+} hydrate, and discuss the measured spectrum of Ce^{3+} in a dilute aqueous solution (1.80 mM of $CeCl_3$ in

20 mM HCl)[35]. Ce^{3+} has a $4f^1$ ground-state configuration, and the parity allowed excitations from the 4f orbitals to the 5d ones give rise to broad absorption bands in the ultraviolet. This aqua ion exhibits flexibility and water exchange in its first hydration shell at 300 K. A previous work by Lindqvist-Reis *et al.*[35] measured and theoretically analyzed the absorption spectrum of the ion and its chloro-derivatives, using crystal structures as model compounds. They observed that both the local symmetry of the coordinated water molecules and their number (9 or 8) around the Ce^{3+} ion considerably influences the positions and the intensities of the absorption bands. In that study, single-point calculations were performed and to match the experimental UV-vis spectra, a chosen phenomenological broadening was applied.

The obtention of a realistic spectrum is conditioned by the selection and the number of the representative structures, reflecting geometrical fluctuations of the aqua ion. In this work, we reconstruct the entire spectrum of the aqua ion averaging individual spectra corresponding to a set of configurations derived from MD simulations, being proved a sufficient number have being selected. These simulations utilize previously developed force fields for lanthanoids in water. Geometrical fluctuations due to thermal agitation, provided by MD simulations, contribute to the broadening of absorption bands. This strategy allows us to capture the anharmonicity present in the system, which comes from QM-computed potential energy surfaces used to parameterize the force field.

II. METHODOLOGY AND COMPUTATIONAL PROCEDURE

To construct the electronic spectrum, we adopted a strategy similar to the one previously developed for averaging EXAFS spectra from MD calculations of metal ions in solution[36,37]. Specifically, individual UV-vis absorption spectra were obtained from simulation snapshots and then averaged.

To illustrate the procedure employed, a flowchart has been included in Figure 1

We employed a set of force fields, based on the hydrated ion model[38,39], which has been applied to study the hydration of various trivalent lanthanoids and actinoids in water[40–42]. A flexible and polarizable water model (MCDHO2)[43] was used. Although no specific ion-water potential was developed for Ce^{3+}, we used force fields closely related lanthanoid cations, La^{3+} and Nd^{3+}. Details of these force fields are provided in the Supplementary Material (SM). We leveraged these force fields to simulate the hydration around Ce^{3+}, assuming that the La^{3+},

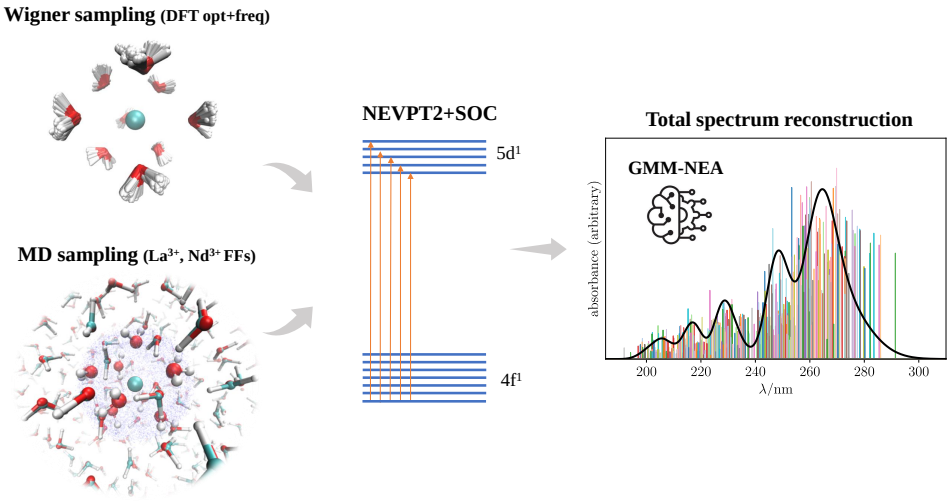

FIG. 1: Schematic representation of the methodology designed to obtain the theoretical spectra.

Nd^{3+}, and Ce^{3+} hydrates exhibit very similar structures for the hydration shells beyond the first one due to their proximity in the Periodic Table[44–46]. Recently, the structure of the first and second hydration shells for the entire series of trivalent lanthanides was investigated by Duvail *et al.*[47], confirming that the second hydration shell exhibits similar structural characteristics across these cations (see Fig. 3 of their work).

MD simulations of La^{3+} and Nd^{3+} surrounded by 1000 water molecules, running for 7 ns in the NVT ensemble with periodic boundary conditions, were conducted. Using an appropriate cutoff radius, approximately 500 clusters per nanosecond of La^{3+} and Nd^{3+} with 9 and 8 water molecules, respectively, were selected. Subsequently, the La and Nd ions were replaced by Ce to perform QM calculations for the vertical transitions between electronic states.

The subsequent step involves QM computations of vertical excitations. This procedure aligns with the methodology used by some of us in a previous study of Ce^{3+}[35], where spin-orbit (SO) coupling was shown to be essential for an accurate QM approach. Scalar relativistic all-electron calculations through the second-order DKH (Douglas-Kroll-Hess) procedure were conducted for computing the vertical excitation energies of Ce^{3+} aqua ions. The energies of the 12 electronic states, corresponding to $4f^1$ and $5d^1$ electronic configurations, were obtained through state-averaged CASSCF calculations. The chosen active space included

one electron distributed over the set of 4f orbitals and 5d orbitals of Ce^{3+} (CASSCF(1,12)). Dynamical electron correlation was incorporated using NEVPT2[48–50]. The spin-orbit coupling was calculated from atomic mean field (AMFI) SO integrals, an approach that proved to be very accurate for valence energy levels[51]. Altogether twelve electronic states corresponding to the electronic states of $4f^1$ (7 states) and $5d^1$ (5 states) configurations were computed.

For the basis set, ma-DKH-def2-QZVPP[52] was used for O and H, while all-electron SARC2-DKH-QZVP[53] was used for Ce. The calculations were further accelerated using the RIJK pseudospectral methods, with the corresponding auxiliary basis sets. This method has been tested and validated in previous works[54,55], showing satisfactory performance even on metals[56–58]. In the case of both octa- and ennea-hydrated ions, 31 and 32 orbitals (corresponding to the oxygen 1s orbitals and the core orbitals of cerium) respectively, were kept frozen in the NEVPT2 correlation step. Some test calculations have been performed including the CPCM solvation model[59]. All QM calculations were performed using the ORCA software[60]. An example of the input is provided in the Supplementary Material (SM).

To build the complete spectrum, a broadening criterion must be assigned. The chosen approach is the Gaussian Mixture Models-Nuclear Ensemble Approach (GMM-NEA) developed by Cerdán and Roca-Sanjuán[21]. This method relies on a probabilistic machine learning technique, GMM, eliminating the need for phenomenological broadening. It can detect outliers from a set of computed vertical excitation energies and oscillator strengths.

III. RESULTS AND DISCUSSION

To incorporate Ce^{3+} specificity in the structures, we optimized the $[Ln(H_2O)_9]^{3+}$ and $[Ln(H_2O)_8]^{3+}$ aqua ions of La^{3+}, Nd^{3+}, and Ce^{3+} at the DFT level using the M06 functional and DEF2-TZVPP basis set, consistent with the level of theory and basis set employed in force field construction. The optimization results are presented in Table I. The average Ln-O distance decreases by -0.040 Å when transitioning from La^{3+} to Ce^{3+} in the enneahydrate cluster and increases by 0.035 Å in the octahydrate when going from Nd^{3+} to Ce^{3+}. For the spectra calculations, we adjusted the snapshots to create "distance-corrected" clusters: we added 0.035 Å to the Nd-O distances in the octahydrate clusters and subtracted 0.040 Å for the La-O bond distances in the enneahydrate clusters. The average Ln-O distances from MD

simulations are also provided in Table I, showing that the outer hydration sphere's effect on this parameter is smaller than a hundredth of an angstrom.

TABLE I: Average Ln-O distances obtained from QM optimizations, from MD simulations and from Wigner sampling. The correction, Δd, from $[La(H_2O)_9]^{3+}$ to $[Ce(H_2O)_9]^{3+}$ and from $[Nd(H_2O)_8]^{3+}$ to $[Ce(H_2O)_8]^{3+}$ comes from the QM optimization results.

Average Ln-O (Å)	$[Ce(H_2O)_9]^{3+}$	$[La(H_2O)_9]^{3+}$	$[Ce(H_2O)_8]^{3+}$	$[Nd(H_2O)_8]^{3+}$
QM optimizations	2.576	2.614	2.541	2.507
Rounded Δd		−0.040		0.035
MD simulations	2.583	2.623	2.540	2.505
Wigner sampling	2.586		2.549	

To assess the consistency of our approach, we generated a sampling of a Q-harmonic Wigner distribution[26] from the QM-optimized geometries of $[Ce(H_2O)_8]^{3+}$ and $[Ce(H_2O)_9]^{3+}$ along with their normal vibrational modes, at 300 K in vacuum. Previous studies have shown that the use of implicit solvation models in geometry optimisation and frequency calculations for such clusters results in minimal changes when compared to vacuum calculations[61,62]. The Ce-O and O-H Wigner distributions were compared with the "distance-corrected" distributions obtained from the octa- and ennea-hydrate in our MD simulations. Table I reveals that the average Ce-O distances differ only by 0.003 Å and 0.009 Å for the ennea- and octa-hydrate, respectively.

To further validate our results, we compared the Ce-O distributions for both hydration numbers, as shown in Figure 2. Both distributions exhibit the maximum at nearly the same position, although the Wigner sampling distribution follows a Gaussian shape (due to the harmonic approximation), while the MD distribution is more asymmetric. These distributions indicate that the main geometrical parameter (Ce-O distance) of the aqua ions presents fluctuations of about 0.4 Å, which clearly produces an spreading in the bands of the spectra obtained from each structure (Figure 3). The O-H distance distributions, included in Figure S3 and Figure S4 of the SM, adopt Gaussian shapes, as expected for the strong O-H bonds, with the MD distribution having a narrower width than the Wigner one. This could be understood on the basis that the O-H bond fluctuations given by the MCDHO2

potential correspond to the fitting of a different potential energy surface to that used for the Wigner distribution. Additionally, the MD simulation account for the interaction between the second hydration shell and the Ce^{3+} aqua ion, while the Wigner distribution corresponds to the aqua ion isolated. Consequently, the solvent's compacting effect, introduced by the MD simulations likely contributes to the narrower O-H distribution in this case.

These values were compared with literature reports. Duvail, Vitorge, and Spezia[44] predicted an average Ce-O distance of 2.50 Å, in agreement with the value proposed by Allen *et al.*[63] in the presence of chloride ions. However, these values are shorter than the 2.569 Å obtained by Migliorati *et al.*[45] using MD approaches. Recent Raman experiments exploring the solvation of Ln(III) ions in perchlorate acid solution proposed similar bond lengths between the cerium ion and the coordinated water molecules (2.565 Å)[46]. The latest results are in line with our proposed values.

The 3300 selected snapshots from MD simulations were all reoriented using *calculate_rmsd.py*[64] with respect to a reference structure to allow the use of the same initial guess orbitals. From these snapshots, individual UV-vis absorption spectra were computed quantum-mechanically to extract excitation energies and oscillator strengths for each structure. The absorption peaks primarily correspond to the parity-allowed 4f to 5d electronic excitations. The next step involves including spectral broadening and convoluting the different signals. As mentioned earlier, the GMM-NEA procedure[21] facilitate the construction of the final spectrum without the need for establishing empirical broadening for each transition line. Figure 3 displays the deconvoluted spectrum resulting from the contributions of individual spectra corresponding to the ennea-hydrate structures (200 among the 3300 are represented), as well as the reconstructed spectrum.

Before analyzing the UV-visible spectrum of the aqueous solution, where the presence of octahydration and enneahydration has been reported[35], we examined the average spectra computed for a given hydration number, either the octahydrate (MD_8w) or the enneahydrate (MD_9w). These spectra can be compared individually with the experimental spectra recorded by Lindqvist-Reis et al.[35] for the crystalline structure doped with Ce^{3+} to obtain an octa- (Exp_solid_8w) or an ennea-coordination (Exp_solid_9w). Figure 4 displays these comparisons. The features in both spectra are quite similar in the general shape and the relative intensities of the different bands, although a red-shifting by about 10 nm in the theoretical results is observed with respect to the most intense experimental peaks (about

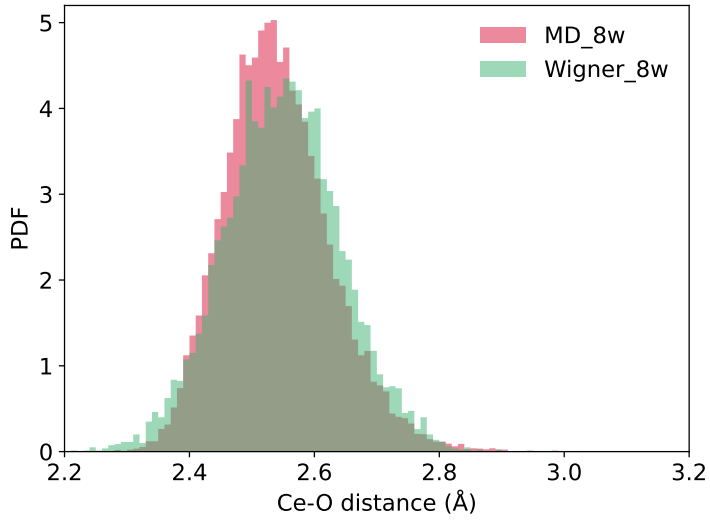

(a) octahydrate

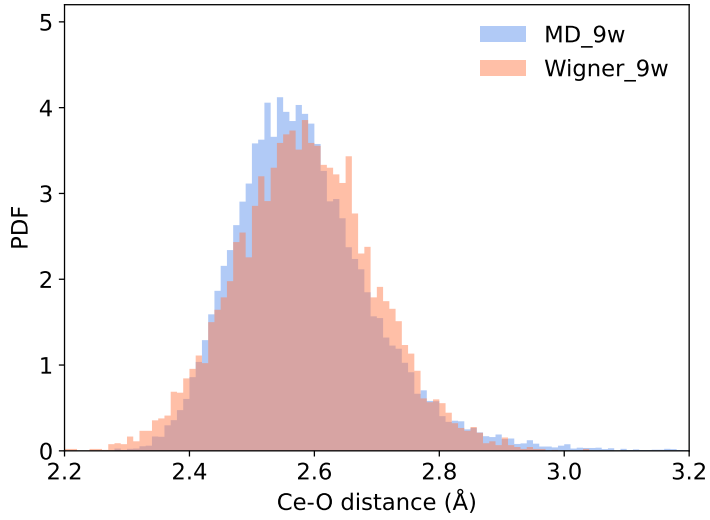

(b) enneahydrate

FIG. 2: Ce-O distance distribution (Probability Density Function) for the octa- (a) and ennea-hydrate (b) structures of Ce^{3+} from MD simulations and Wigner distributions at 300 K.

240 nm and 260 nm for the octa and ennea-coordinated cerium in the cristalline structures). While a match between experimental and theoretical spectra is not expected due to the difference between crystalline and liquid samples, the close similarity must be understood as the fact that the common $[Ce(H_2O)_n]^{3+}$ motif is the main responsible for the electronic

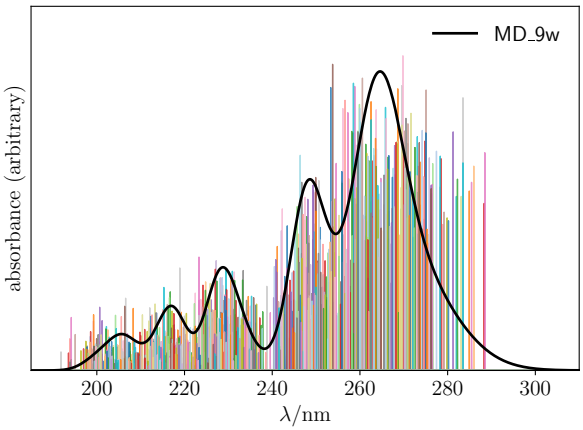

FIG. 3: Computed spectrum of individual snapshots (200 among the 3300 are represented) and average theoretical spectrum corresponding to the $[Ce(H_2O)_9]^{3+}$ aqua ion.

transitions.

The UV-visible spectrum of the $CeCl_3$ aqueous solution[35] (Exp_aq) is presented alongside average spectra obtained from MD simulations corresponding to the ennea- (MD_9w) and octa-coordination (MD_8w) in Figure 5. The small experimental peak at $\sim$ 300 nm was assigned by the authors to the octa-coordination[35]. This assignment is corroborated by the theoretical spectrum of the octahydrate where an intense signal appears at this wavelength, whereas no peak is present in the case of the enneahydrate. The previous comparison of solid samples, where the octa- and ennea-coordination can be analyzed separately, also corroborates this assignment. The significant intensity disparity between the experimental and simulated octahydrate spectra suggests that the aqueous solution contains a minor fraction of Ce^{3+} aqua ion under this specific coordination. Conversely, the simulated spectrum for enneahydration closely resembles the experimental spectrum with a slight red shift of approximately 10 nm, indicating that the enneahydrated aqua ion predominates in the solution at 300 K, suggesting an equilibrium between both aqua ions.

In addition to the solvent effects induced by outer solvation shells on the aqua ion structure, we have explored the solvent effects on the electronic spectrum due to the inclusion of a continuum solvation model, as the CPCM method[65]. Figure S5 in the SM shows the spectra computed with and without the inclusion of the dielectric medium for a set of 500 structures taken from 1 ns of MD simulation. The results indicate minor alteration in spectrum shapes. Bearing in mind that electronic states involved in the transitions correspond to

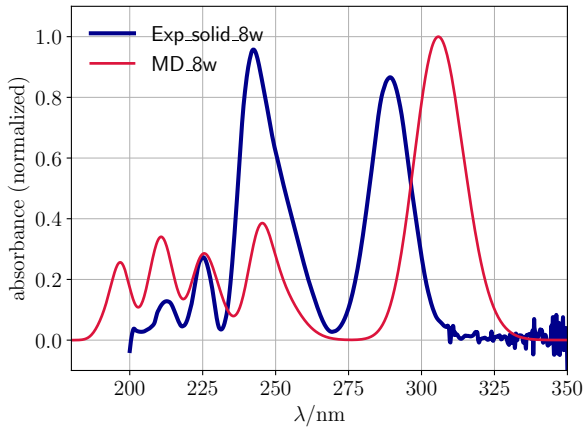

(a) octahydrate

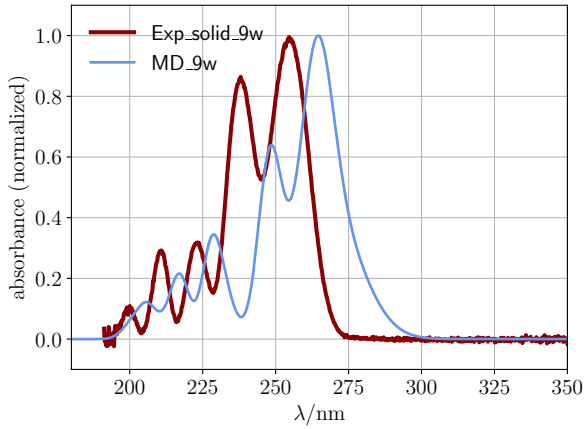

(b) enneahydrate

FIG. 4: (a) Experimental spectra of crystalline cerium with octa-coordination (Exp_solid_8w) and the average theoretical spectrum of the $[Ce(H_2O)_8]^{3+}$ aqua ion (MD_8w). (b) Experimental spectra of crystalline cerium with ennea-coordination (Exp_solid_9w) and the average theoretical spectrum of the $[Ce(H_2O)_9]^{3+}$ aqua ion (MD_9w).

orbitals centered on the Ce^{3+} center, and assuming that the multipole charge distribution of the wavefunctions remains relatively unchanged from ground to excited states, the solvent reaction field induces similar effects on both states.

The analysis of the temperature influence on this equilibrium represents a significant step towards understanding Ce^{3+} hydration behavior. Experimental investigations conducted by Lindqvist-Reis *et al.*[35] recorded absorption spectra of Ce^{3+} in diluted aqueous solutions

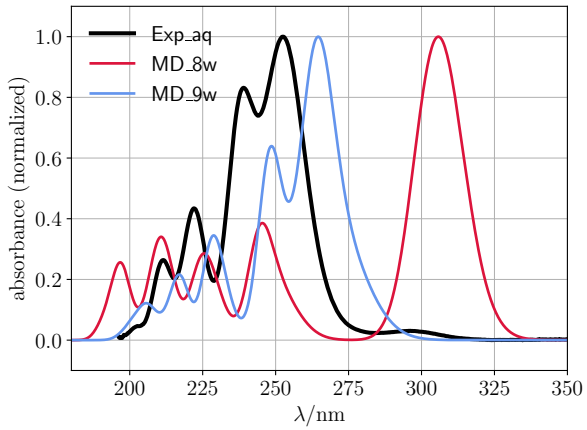

FIG. 5: Experimental spectrum of Ce^{3+} in solution (Exp_aq), average theoretical spectrum of enneahydrated Ce^{3+} (MD_9w) and average theoretical spectrum of octahydrated Ce^{3+} (MD_8w).

across temperatures ranging from 10 °C to 90 °C. Figure 6 displays the spectra corresponding to the lowest (10 °C) and highest (90 °C) temperatures. With increasing temperature, the population of the octahydrate aqua ion rises. Lindqvist-Reis *et al.*[35] proposed molar fractions of this octahydrate aqua ion to be 0.12 and 0.30 at 10 °C and 90 °C, respectively. Simulated spectra at these temperatures (MD_mix) were computed by averaging electronic spectra, maintaining the octa- and ennea-hydrate ratio consistent with the experimental data. To facilitate comparison of features, the simulated spectra were blue-shifted by 1590 cm^{-1} to align more closely with the experimental spectra. In Figure 6, a notable agreement between experimental and simulated spectra is observed, particularly in the 200 nm to 280 nm range, where band intensities and relative positions are consistently reproduced. Although the intensity of the peak near 300 nm is overestimated for both temperatures, consistent with observations in the spectrum corresponding to the octa-coordinated Ce-doped crystal and its simulated counterpart (see Figure 4a), the relative intensity changes across the bands remain consistent between the experimental and simulated spectra. These temperature-related findings reinforce the confidence in the statistical and QM methodologies employed to construct the UV-vis spectra and affirm the existence of a chemical equilibrium in solution between ennea- and octa-coordination. An additional test of the performance of our methodology is to compare the absolute intensity against the experimental spectrum, instead of the normalized absorbance. Cerdán and Roca-Sanjuán[21] show how to obtain the absorption cross

section ($\sigma(E)$) from a set of energies and oscillator strengths in GMM-NEA method. This is what has been represented in the previous figures normalizing the intensity to the highest one. σ is related to the molar extintion coefficient ($\epsilon(E)$) as $\epsilon(E) = \sigma(E)N_A/ln(10)$. Figure S6 shows the comparison of the experimental spectrum with the theoretical ones without normalization. There is a 2 factor for the variation of ϵ with wavelength when comparing experiment and theory, but the relative intensity of the maxima does not seem to be affected by the coordination number. This indicates that the absorption cross section is independent of the ion coordination. In addition, Figure S7 shows a comparison of the octa and ennea coordination mixtures using the observed mole fractions at 30ºC, again without normalization, and blue-shifted to match the maximum of the most intense band.

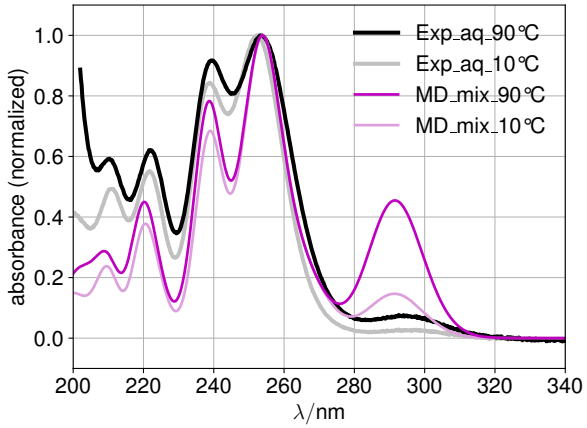

FIG. 6: Experimental absorption spectra at 10 °C and 90 °C and the combination of MD_8w and MD_9w theoretical spectra at the respective molar fractions. The simulated spectra have been blue-shifted by 1590 cm^{-1} to maximize the overlap with the experimental data.

Once a satisfactory reproduction of the experimental spectrum has been achieved, one should examine how convergence was attained with respect to the number of structures used in the statistical average spectrum. The evolution of the spectrum with the number of snapshots is illustrated in Figure S8 and Figure S9 of the SM for the cases of the Ce^{3+} octahydrate and enneahydrate, respectively. In both cases, a visual inspection reveals that spectra with more than 1000 structures closely match.

To quantitatively establish convergence, we employed the relative integral change (RIC) method proposed by Xue, Barbatti, and Dral[66]. A detailed description of this procedure can

be found in the SM, and Figure S10 illustrates how the RIC index reaches an appropriate threshold when 1000 structures are included in the spectrum reconstruction.

While achieving a good reproduction of the shape and position of bands in experimental spectra, exploring alternative methods to obtain an ensemble of structures without relying on a force field for MD computations is worthwhile. One such approach is Wigner sampling[26–28]. The theoretical spectra obtained at 300 K from both MD simulations and Wigner sampling for ennea- and octa-hydrates are depicted in Figure 7. For the octa-aqua ion, the spectra show similar band shapes and positions, with the most intense peak exhibiting a slight shift of approximately 5 nm. In contrast, the spectrum from Wigner sampling for the enneahydrate ion displays slightly reduced intensity in the lower wavelength region, and the most intense peak is also shifted. Despite the very similar Ce-O distances (see Table I and Figure 2), significant differences are observed in the O-H distributions, detailed in the SM (see Figure S3 and Figure S4). The orientation of water molecules relative to the central cation has been identified to significantly influence the relative intensities of vertical transitions in Ce^{3+} aqua ions, as highlighted in the previous study by Lindqvist-Reis *et al.*[35]. Thus, discrepancies between the theoretical spectra from MD simulations and Wigner sampling methods may be attributed to differing treatments of vibrational water modes. Furthermore, these discrepancies may be also attributed to the fact that in MD simulations the interactions of the first- and second-hydration shell are described, whereas in the Wigner case only the first hydration shell is taken into account.

It is crucial to highlight that deriving spectra from MD simulations typically necessitates access to specific force fields and subsequent classical MD simulations, or alternatively, performing ab initio MD simulations. In contrast, computing Wigner spectra requires only the geometry optimization of the cluster and its second derivatives. This data is sufficient to generate a statistical sampling using the Wigner method, which is computationally less demanding compared to classical or ab initio MD simulations.

IV. CONCLUDING REMARKS

In summary, this study demonstrates the successful integration of a well-balanced statistical distribution of structures obtained from MD simulations with highly-correlated relativistic xQM computations of UV-vis spectra in Ce^{3+}-containing aqueous solutions. The

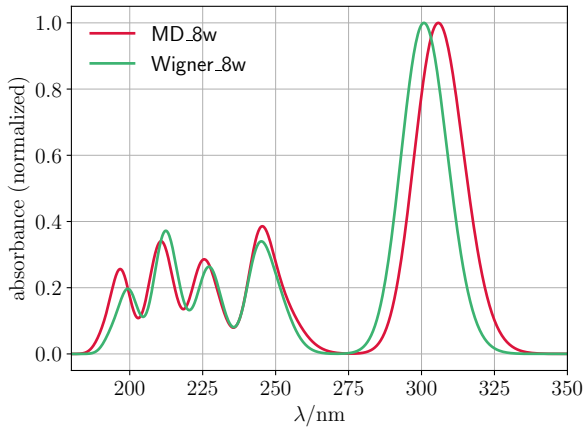

(a) octahydrate

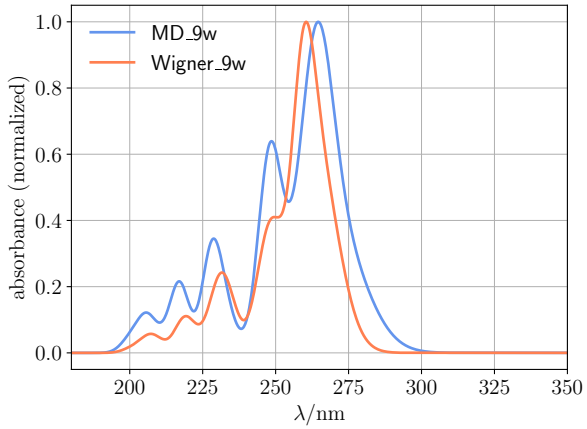

(b) enneahydrate

FIG. 7: Average theoretical spectra for the $[Ce(H_2O)_8]^{3+}$ (a) $[Ce(H_2O)_9]^{3+}$ (b) in solution obtained from the MD simulations (MD_8w and MD_9w) and average theoretical spectra derived from a Wigner sampling (Wigner_8w and Wigner_9w) at 300 K.

flexibility of the aqua ion, captured by the force field, is pivotal in accurately reconstructing the entire spectrum from numerous individual spectra. Spectrum broadening is attributed, in part, to geometrical fluctuations influencing both the position and intensity of transition lines, as illustrated in Figure 3. The inherent statistical distribution of numerous vertical transitions effectively reproduces band shapes through broadening based on statistical distribution rather than a parametric criterion. Additionally, the study explores an alternative method using Wigner sampling, which produces electronic spectra similar to those derived from MD simulations. This approach, combining Wigner sampling with the GMM-NEA

method for spectrum construction, offers insights applicable to addressing various chemical challenges where such a combination proves advantageous.

SUPPLEMENTARY MATERIAL

Supplementary Material includes a description of the MCDHO2 model and the force field employed for the ion-water and water-water interactions. O-H distance distributions of the MD simulations. ORCA input file for electronic spectrum computation. Comparison of theoretical spectra computed with or without a continuum solvation model. Comparison of the theoretical and experimental spectra using absolute intensities in terms of molar extinction coefficient. Test of convergence of the spectra computed from a given number of snapshots. Evolution of the RIC convergence index with the number of structures used for averaging using GMM-NEA method.

ACKNOWLEDGMENTS

We thank Dr. J. M. Martínez, University of Seville, for helpful comments and suggestions and P. Lindqvist-Reis for the raw experimental data. This document is the result of the I+D+i research project PGC2018-099366-B-I00 funded by the Ministerio de Ciencia e Innovación/Agencia Estatal de Investigación /10.13039/501100011033/ and by ERDF a way of making Europe. GRH thanks for a Ph.D. grant (PIF, VI PPIT-US) to the University of Seville. FR and VV acknowledge the "Groupement de recherche" GDR 2035 SolvATE, along with support from the PIA ANR project CaPPA (ANR-11-LABX-0005-01), the I-SITE ULNE projects OVERSEE and MESONM International Associated Laboratory (LAI) (ANR-16-IDEX-0004), the French Ministry of Higher Education and Research, region Hauts de France council and European Regional Development Fund (ERDF) project CPER CLIMIBIO, WaveTech and the French national supercomputing facilities (grants DARI A0130801859, A0110801859).

Ce(III) UV-vis spectrum

AUTHOR DECLARATIONS

Conflict of Interest

The authors have no conflicts to disclose.

Author Contributions

Gema Raposo-Hernández: Data curation; Formal analysis; Investigation; Software; Visualization. Rafael R. Pappalardo: Data curation; Investigation; Visualization; Methodology; Software; Validation. Florent Réal: Conceptualization; Investigation; Visualization; Supervision; Software. Valérie Vallet: Conceptualization; Investigation; Methodology; Software; Visualization; Resources; Writing – review & editing. Enrique Sánchez Marcos: Conceptualization; Funding acquisition; Validation; Visualization; Writing - first draft; Writing – review & editing.

V. DATA AVAILABILITY

The data that support the findings of this study are available within the article and its supplementary material.

REFERENCES

[1]H.-H. Perkampus, *UV-vis Spectroscopy and its Applications* (Springer-Verlag, 1992).

[2]C. Reichardt, *Solvents and Solvent Effects in Organic Chemistry* (Wiley-VCH, Weinheim, 2004).

[3]E. Gallo, E. Gorelov, A. Guda, A. Bugaev, F. Bonino, E. Borfecchia, G. Ricchiardi, D. Gianolio, S. Chavan, and C. Lamberti, "Effect of molecular guest binding on the d–d transitions of Ni^{2+} of CPO-27-Ni: A combined UV–vis, resonant-valence-to-core X-ray emission spectroscopy, and theoretical study," Inorg. Chem. **56**, 14408–14425 (2017).

[4]G. Ganguly, Z. Havlas, and J. Michl, "Ab initio calculation of UV–vis absorption of parent Mg, Fe, Co, Ni, Cu, and Zn metalloporphyrins," Inorg. Chem. **63**, 10127–10142 (2024).

[5]A. Stoïanov, J. Champion, and R. Maurice, "UV–vis absorption spectroscopy of polonium(IV) chloride complexes: An electronic structure theory study," Inorg. Chem. **58**, 7036–7043 (2019).

[6]C. Danilo, V. Vallet, J.-P. Flament, and U. Wahlgren, "Spin-orbit configuration interaction study of the electronic structure of the $5f^2$ manifold of U^{4+} and the 5f manifold of U^{5+}," J. Chem. Phys. **128**, 154310 (2008).

[7]M. H. Palmer, T. Ridley, S. V. Hoffmann, N. C. Jones, M. Coreno, M. de Simone, C. Grazioli, T. Zhang, M. Biczysko, A. Baiardi, and K. Peterson, "Interpretation of the photoelectron, ultraviolet, and vacuum ultraviolet photoabsorption spectra of bromobenzene by ab initio configuration interaction and DFT computations," J. Chem. Phys. **143**, 164303 (2015).

[8]D. T. Richens, *The Chemistry of Aqua Ions* (John Wiley, New York, 1997).

[9]V. Barone, R. Impronta, and N. Rega, "Quantum mechanical computations and spectroscopy: From small rigid molecules in the gas phase to large flexible molecules in solution," Acc. Chem. Res. **41**, 605–616 (2008).

[10]C. Danilo, V. Vallet, J.-P. Flament, and U. Wahlgren, "Effects of the first hydration sphere and the bulk solvent on the spectra of the f^2 isoelectronic actinide compounds: U^{4+}, NpO_2^+, and PuO_2^{2+}," Phys. Chem. Chem. Phys. **12**, 1116–1130 (2010).

[11]T. Zuehlsdorff and C. Isborn, "Modeling absorption spectra of molecules in solution," Int. J. Quantum Chem. **119**, e25719 (2019).

[12]R. Sarkar, P.-F. Loos, M. Boggio-Pasqua, and D. Jacquemin, "Assessing the performances of CASPT2 and NEVPT2 for vertical excitation energies," J. Chem. Theory Comput. **18**, 2418–2436 (2022).

[13]G. A. Worth, H.-D. Meyer, H. Köppel, L. Cederbaum, and I. Burghardt, "Using the mctdh wavepacket propagation method to describe multimode non-adiabatic dynamics," Int. Rev. Phys. Chem. **27**, 569–606 (2008).

[14]J. Segarra-Martí, F. Segatta, T. A. Mackenzie, A. Nenov, I. Rivalta, M. J. Bearpark, and M. Garavelli, "Modeling multidimensional spectral lineshapes from first principles: application to water-solvated adenine," Faraday Discuss. **221**, 219–244 (2020).

[15]H. Oher, F. Réal, T. Vercouter, and V. Vallet, "Investigation of the luminescence of $[UO_2X_4]^{2-}$ (X = Cl, Br) complexes in the organic phase using time-resolved laser-induced fluorescence spectroscopy and quantum chemical simulations," Inorg. Chem. **59**, 5896–5906

(2020).

[16]F. Egidi, D. B. Williams-Young, A. Baiardi, J. Bloino, G. Scalmani, M. J. Frisch, X. Li, and V. Barone, "Effective inclusion of mechanical and electrical anharmonicity in excited electronic states: VPT2-TDDFT route," J. Chem. Theory Comput. **13**, 2789–2803 (2017).

[17]A. Baiardi, J. Bloino, and V. Barone, "General time dependent approach to vibronic spectroscopy including franck–condon, herzberg–teller, and duschinsky effects," J. Chem. Theory Comput. **9**, 4097–4115 (2013).

[18]J. Bloino, M. Biczysko, O. Crescenzi, and V. Barone, "Integrated computational approach to vibrationally resolved electronic spectra: Anisole as a test case," J. Chem. Phys. **128**, 244105 (2008).

[19]J.-L. Chang, H.-Y. Chen, and Y.-J. Huang, "Reassignment of the photoelectron spectrum of methylketene using a hybrid model of harmonic and anharmonic oscillators to compute franck–condon factors," ACS Omega **8**, 40685–40694 (2023).

[20]D. Madsen, O. Christiansen, P. Norman, and C. König, "Vibrationally resolved emission spectra of luminescent conjugated oligothiophenes from anharmonic calculations," Phys. Chem. Chem. Phys. **21**, 17410–17422 (2019).

[21]L. Cerdán and D. Roca-Sanjuán, "Reconstruction of nuclear ensemble approach electronic spectra using probabilistic machine learning," J. Chem. Theory Comput. **18**, 3052–3064 (2022).

[22]N. Rojas-Valencia, S. Gómez, T. Giovannini, C. Cappelli, A. Restrepo, and F. Núñez-Zarur, "Water maintains the UV–vis spectral features during the insertion of anionic naproxen and ibuprofen into model cell membranes," J. Phys. Chem. B **127**, 2146–2155 (2023).

[23]P. P. Fehér, A. Madarász, and A. Stirling, "Multiscale modeling of electronic spectra including nuclear quantum effects," J. Chem. Theory Comput. **17**, 6340–6352 (2021).

[24]S. Di Grande, I. Ciofini, C. Adamo, M. Pagliai, and G. Cardini, "Absorption spectra of flexible fluorescent probes by a combined computational approach: Molecular dynamics simulations and time-dependent density functional theory," J. Phys. Chem. A **126**, 8809–8817 (2022).

[25]M. Barbatti, A. J. A. Aquino, and H. Lischka, "The UV absorption of nucleobases: semi-classical ab initio spectra simulations," Phys. Chem. Chem. Phys. **12**, 4959–4967 (2010).

[26]R. Crespo-Otero and M. Barbatti, "Spectrum simulation and decomposition with nuclear ensemble: formal derivation and application to benzene, furan and 2-phenylfuran," Theor. Chem. Acc. **131**, 1237 (2012).

[27]E. Wigner, "On the quantum correction for thermodynamic equilibrium," Phys. Rev. **40**, 749–759 (1932).

[28]A. Saiz-Lopez, S. P. Sitkiewicz, D. Roca-Sanjuán, J. M. Oliva-Enrich, J. Z. Dávalos, R. Notario, M. Jiskra, Y. Xu, F. Wang, C. P. Thackray, *et al.*, "Photoreduction of gaseous oxidized mercury changes global atmospheric mercury speciation, transport and deposition," Nat. Commun. **9**, 4796 (2018).

[29]J. Cerezo, D. Aranda, F. J. Avila Ferrer, G. Prampolini, and F. Santoro, "Adiabatic-molecular dynamics generalized vertical hessian approach: a mixed quantum classical method to compute electronic spectra of flexible molecules in the condensed phase," J. Chem. Theory Comput. **16**, 1215–1231 (2020).

[30]A. Segalina, J. Cerezo, G. Prampolini, F. Santoro, and M. Pastore, "Accounting for vibronic features through a mixed quantum-classical scheme: Structure, dynamics, and absorption spectra of a perylene diimide dye in solution," J. Chem. Theory Comput. **16**, 7061–7077 (2020).

[31]S. Gómez, T. Giovannini, and C. Cappelli, "Multiple facets of modeling electronic absorption spectra of systems in solution," ACS Physical Chemistry Au **3**, 1–16 (2023).

[32]T. J. Zuehlsdorff, P. D. Haynes, M. C. Payne, and N. D. M. Hine, "Predicting solvatochromic shifts and colours of a solvated organic dye: The example of Nile red," J. Chem. Phys. **146**, 124504 (2017).

[33]O. B. Malcıoğlu, A. Calzolari, R. Gebauer, D. Varsano, and S. Baroni, "Dielectric and thermal effects on the optical properties of natural dyes: A case study on solvated cyanin," J. Am. Chem. Soc. **133**, 15425–15433 (2011).

[34]X. Ge, I. Timrov, S. Binnie, A. Biancardi, A. Calzolari, and S. Baroni, "Accurate and inexpensive prediction of the color optical properties of anthocyanins in solution," J. Phys. Chem. A **119**, 3816–3822 (2015).

[35]P. Lindqvist-Reis, F. Réal, R. Janicki, and V. Vallet, "Unraveling the ground state and excited state structures and dynamics of hydrated Ce^{3+} ions by experiment and theory," Inorg. Chem. **57**, 10111–10121 (2018).

[36]P. J. Merkling, A. Muñoz-Páez, and E. Sánchez Marcos, "Exploring the capabilities of x-ray absorption spectroscopy for determining the structure of electrolyte solutions; computed spectra for Cr^{3+} or Rh^{3+} in water based on molecular dynamics," J. Am. Chem. Soc. **124**, 10911–10920 (2002).

[37]G. Raposo-Hernández, J. M. Martínez, R. R. Pappalardo, C. Den Auwer, and E. Sánchez Marcos, "A coupled EXAFS-molecular dynamics study on PuO_2^+ and NpO_2^+ hydration: The importance of electron correlation in force-field building," Inorg. Chem. **61**, 8703–8714 (2022).

[38]J. M. Martínez, R. R. Pappalardo, and E. Sánchez Marcos, "First-principles ion-water interaction potentials for highly charged monoatomic cations.computer simulations of Al^{3+},Mg^{2+} and Be^{2+}," J. Am. Chem. Soc. **121**, 3175–3184 (1999).

[39]E. Galbis, J. Hernández-Cobos, C. den Auwer, C. Le Naour, D. Guillaumont, E. Simoni, R. R. Pappalardo, and E. Sánchez Marcos, "Solving the hydration structure of the heaviest actinide aqua ion known: The californium (III) case," Angew. Chem. Int. Ed. **122**, 3899–3903 (2010).

[40]N. Morales, E. Galbis, J. M. Martínez, R. R. Pappalardo, and E. Sánchez Marcos, "Identifying coordination geometries of metal aqua ions in water: Application to the case of lanthanoid and actinoid hydrates," J. Phys. Chem. Lett. **7**, 4275–4280 (2016).

[41]D. Z. Caralampio Minguez, *Looking for Synergies in Solution Chemistry Between First-principles Intermolecular Potentials and EXAFS and XANES Spectroscopies*, Ph.D. thesis, Universidad de Sevilla (https://idus.us.es/handle/11441/78598) (2018).

[42]R. R. Pappalardo, D. Caralampio, J. M. Martínez, and E. Sánchez Marcos, "Hydration structure of the elusive Ac(III) aqua ion: Interpretation of X-ray absorption spectroscopy (XAS) spectra on the basis of molecular dynamics (MD) simulations," Inorg. Chem. **58**, 2777–2783 (2019).

[43]A. Villa, B. Hess, and H. Saint-Martin, "Dynamics and structure of Ln(III) aqua ions: A Comparative Molecular Dynamics study using ab initio based flexible and polarizable model potentials," J. Phys. Chem. B **113**, 7270–7281 (2009).

[44]M. Duvail, P. Vitorge, and R. Spezia, "Building a polarizable pair interaction potential for lanthanoids(III) in liquid water: A molecular dynamics study of structure and dynamics of the whole series," J. Chem. Phys. **130**, 104501 (2009).

[45]V. Migliorati, A. Serva, F. M. Terenzio, and P. D'Angelo, "Development of Lennard-Jones and Buckingham Potentials for Lanthanoid Ions in Water," Inorg. Chem. **56**, 6214–6224 (2017).

[46]W. W. Rudolph and G. Irmer, "Raman spectroscopic characterization of light rare earth ions: La^{3+} , Ce^{3+}, Pr^{3+}, Nd^{3+} and Sm^{3+} – hydration and ion pair formation," Dalton Trans. **46**, 4235–4244 (2017).

[47]M. Duvail, D. Moreno Martinez, L. Žiberna, E. Guillam, J.-F. Dufrêche, and P. Guilbaud, "Modeling lanthanide ions in solution: A versatile force field in aqueous and organic solvents," J. Chem. Theory Comput. **20**, 1282–1292 (2024).

[48]C. Angeli, R. Cimiraglia, S. Evangelisti, T. Leininger, and J.-P. Malrieu, "Introduction of n-electron valence states for multireference perturbation theory," J. Chem. Phys. **114**, 10252–10264 (2001).

[49]C. Angeli, R. Cimiraglia, and J.-P. Malrieu, "N-electron valence state perturbation theory: a fast implementation of the strongly contracted variant," Chem. Phys. Lett. **350**, 297–305 (2001).

[50]C. Angeli, R. Cimiraglia, and J.-P. Malrieu, "n-electron valence state perturbation theory: A spinless formulation and an efficient implementation of the strongly contracted and of the partially contracted variants," J. Chem. Phys. **117**, 9138–9153 (2002).

[51]S. Knecht, M. Repisky, H. J. A. Jensen, and T. Saue, "Exact two-component hamiltonians for relativistic quantum chemistry: Two-electron picture-change corrections made simple," J. Chem. Phys. **157**, 114106 (2022).

[52]F. Weigend, M. Häser, H. Patzelt, and R. Ahlrichs, "RI-MP2: optimized auxiliary basis sets and demonstration of efficiency," Chem. Phys. Lett. **294**, 143–152 (1998).

[53]D. Aravena, F. Neese, and D. A. Pantazis, "Improved segmented all-electron relativistically contracted basis sets for the lanthanides," J. Chem. Theory Comput. **12**, 1148–1156 (2016).

[54]J. M. Guevara-Vela, T. Rocha-Rinza, and A. M. Pendás, "Performance of the RI and RI-JCOSX approximations in the topological analysis of the electron density," Theor. Chem. Acc. **136**, 57 (2017).

[55]C. Naim, P. Besalú-Sala, R. Zaleśny, J. M. Luis, F. Castet, and E. Matito, "Are accelerated and enhanced wave function methods accurate to compute static linear and nonlinear optical properties?" J. Chem. Theory Comput. **19**, 1753–1764 (2023).

[56]S. Klokishner, O. Reu, J. Noack, R. Schlögl, and A. Trunschke, "Experimental study and modeling of the UV–vis and infrared spectra of the [VO(O2)Hheida]- complex dissolved in water," J. Phys. Chem. A **121**, 7157–7164 (2017).

[57]J. M. A. Alves, I. G. R. Domingos, and M. T. de Oliveira, "Accelerating computations of organometallic reaction energies through hybrid basis sets," Inorg. Chem. Front. **10**, 2262–2267 (2023).

[58]S. Klokishner and O. Reu, "Modeling of spin crossover in iron(II) complexes with N4S2 coordination," J. Phys. Chem. C **123**, 19984–19990 (2019).

[59]M. Garcia-Ratés and F. Neese, "Effect of the solute cavity on the solvation energy and its derivatives within the framework of the gaussian charge scheme," Journal of Computational Chemistry **41**, 922–939 (2020), https://onlinelibrary.wiley.com/doi/pdf/10.1002/jcc.26139.

[60]F. Neese, "Software update: The orca program system—version 5.0," Wiley Interdiscip. Rev. Comput. Mol. Sci. **12**, e1606 (2022).

[61]J. M. Martínez, R. R. Pappalardo, and E. S. Marcos, "Study of the Ag^+ hydration by means of a semicontinuum quantum-chemical solvation model," J. Phys. Chem. A **101**, 4444–4448 (1997).

[62]J. M. Martínez, R. R. Pappalardo, E. Sánchez Marcos, B. Mennucci, and J. Tomasi, "Analysis of the opposite solvent effects caused by different solute cavities on the metal-water distance of monoatomic cation hydrates," J. Phys. Chem. B **106**, 1118–1123 (2002).

[63]P. G. Allen, J. J. Bucher, D. K. Shuh, N. M. Edelstein, and I. Craig, "Coordination chemistry of trivalent lanthanide and actinide ions in dilute and concentrated chloride solutions," Inorg. Chem. **39**, 595–601 (2000).

[64]J. Kromann, "Calculate Root-mean-square deviation (RMSD) of two molecules, https://github.com/charnley/rmsd,".

[65]J. Tomasi, B. Mennucci, and R. Cammi, "Quantum mechanical continuum solvation models," Chem. Rev. **105**, 2999–3094 (2005).

[66]B.-X. Xue, M. Barbatti, and P. O. Dral, "Machine learning for absorption cross sections," J. Phys. Chem. A **124**, 7199–7210 (2020).